TUDelft

Delft University of Technology

Dynamic behaviour of wave packets in turbulent jets

Raiola, Marco; Ragni, Daniele

Citation (APA)
Raiola, M., & Ragni, D. (2019). Dynamic behaviour of wave packets in turbulent jets. In C. J. Kähler, R. Hain, S. Scharnowski, & T. Fuchs (Eds.), *Proceedings of the 13th International Symposium on Particle Image Velocimetry: 22-27 July, Munich, Germany* (pp. 1478-1487). Universitat der Bundeswehr Munchen. https://doi.org/10.18726/2019_3

Important note
To cite this publication, please use the final published version (if applicable).
Please check the document version above.

Dynamic behaviour of wave packets in turbulent jets

Marco Raiola[1]*, Daniele Ragni[2]

[1] University Carlos III of Madrid, Aerospace Engineering Group, Leganes, Spain

[2] Delft University of Technology, AWEP Department, Delft, Netherlands

* mraiola@ing.uc3m.com

Abstract

The present study proposes a data-driven strategy to extract the dynamics of wave-packets from low-speed velocity field measurements. The flow field under study is a subsonic turbulent round jet at $Re = 33000$, measured over a 20-nozzle-diameters domain in the axial direction using low-repetition-rate planar Particle Image Velocimetry. The turbulent features in the jet have been extracted by Proper Orthogonal Decomposition of the jet velocity field over the whole extension of the domain. The modes produced describe the evolution of the turbulent features in the axial and radial directions of the jet. The temporal evolution of turbulent flow structures and the associated pressure fluctuations, which are not directly accessible from the low-speed measurements, have been estimated using an advection-based Galerkin projection model. The extracted velocity/pressure modes describe a set of modulated waves in the axial direction, which shares many similarities with wave-packets already observed in literature. This behaviour suggests that the employed strategy is effective in retrieving the dynamics of wave-packets extending over the entire measurement domain, paving the way to the estimation of their sound emission from low-speed measurements.

1 Introduction

Despite being one of the most studied problems in aeroacoustics, still several aspects of jet-noise eludes the understanding of the research community. While Lighthill (1952) identified the random turbulent eddies in the subsonic jet shear layer as the main source of noise, literature agrees that coherent structures advecting with the flow, generally named wave-packets, play a principal role in the sound radiation (Jordan and Gervais, 2008). These structures generally account for a small fraction of the total turbulent kinetic energy of the flow (Michalke and Fuchs, 1975; Mankbadi and Liu, 1984); nevertheless they emit sound more efficiently than the smaller scales of turbulence, resulting in a strong contribution to noise despite their low energy content. Crighton and Huerre (1990) showed that the sound radiated by a subsonically advecting coherent structure is related to the non-homogeneity of these coherent structures in the advection direction, in particular to their modulation in the axial direction of the jet, which allows high acoustic efficiency at low zenithal angles. It is widely accepted by the aeroacoustic community, even in the absence of conclusive proofs, that the shock-free jet noise is produced by two distinct sources: an omnidirectional incoherent source associated to fine-scale turbulence and a coherent source associated with wave-packets radiating mostly at small zenithal angles (Tam et al., 2008). A large effort from the aeroacoustics community is currently directed towards the identification of the wave-packets (Jordan and Colonius, 2013). The major difficulties on this side reside in the low energetic content of these features and their temporal intermittency, which makes difficult to target them without an external forcing of the jet (Crow and Champagne, 1971). Recently several attempts have been made to model the wave-packet distribution of turbulence exploiting advanced post-processing techniques (Schmidt et al., 2017): these techniques are especially well-suited to capture the intrinsic non-linear dynamic behaviour of these structures (Jaunet et al., 2017), paving the way to further studies which may shed light on their role in jet-noise emission.

The present study is directed towards finding this link, analyzing a turbulent subsonic axial-symmetric jet at $Re = 33000$. The study aims at characterizing the jet and the turbulent features in it before attempting to extract information on the wave-packets. The velocity field has been measured in the symmetry plane of the jet with Particle Image Velocimetry. The measured velocity fields have been analyzed to extract information on the time-averaged jet profiles. Proper Orthogonal Decomposition has been applied to identify the most

energetic turbulent features in the jet. Based on this decomposition a Reduced Order Model of the wave-packets dynamics, including both velocity and hydrodynamic pressure fluctuations, has been obtained by means of a Galerkin projection approach.

2   Experimental setup

A turbulent subsonic jet at $Re = V_J D/\nu = 33000$ has been studied. The jet issues from an axial-symmetric nozzle with exit diameter $D = 20mm$ with a jet exit velocity $V_J = 25m/s$. Jet seeding is obtained by feeding into the stagnation chamber air premixed with DEHS droplets (with approximately $1\mu m$ diameter) produced with a Laskin nozzle. The jet is confined in a closed environment with approximate dimensions $50D \times 50D \times 50D$ in order to have similar particle concentration inside and outside the jet. Planar flow field measurements in the symmetry plane of the jet are obtained using Particle Image Velocimetry (PIV). Illumination is provided by a double-pulsed Quantel Evergreen Nd:Yag Laser (200mJ/pulse at 15Hz). A set of 3 sCMOS Andor Zyla 5.5Mpixels sCMOS cameras aligned along the jet axis direction is employed to image the flow field. The field of view spanned by the 3 cameras is roughly equivalent to an area of $6D \times 20D$. A sketch of the experimental setup is provided in Fig. 1. The particle images have been cross-correlated using a multi-pass image deformation algorithm (Scarano, 2001). The final interrogation window is 40x40 pixels with 75% overlap, corresponding to a vector spacing of 0.029D in the field of view. The final ensemble consists of 2600 velocity fields sampled at 10Hz repetition rate.
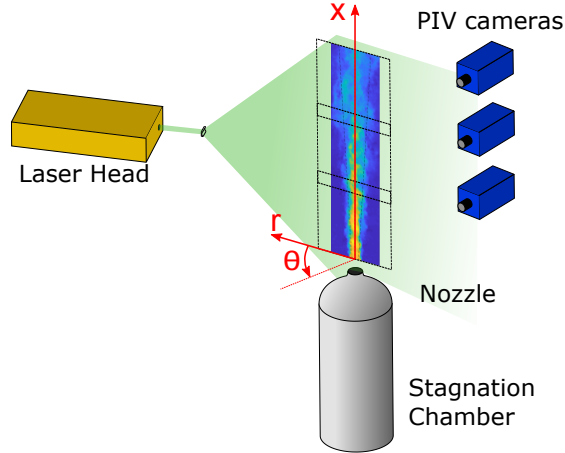

Figure 1: A sketch of the experimental setup.

3   Proper orthogonal decomposition

The Proper Orthogonal Decomposition (POD, Berkooz et al. 1993) is a mathematical procedure which identifies a set of orthonormal eigenfunctions which provide the most compact representation, in a least-square sense, of a set of observations. For the porpouses of this work, let the observations correspond to the instantaneous velocity fields measured with PIV at different time steps, which leads to the bi-orthogonal POD definition (Aubry, 1991). The velocity field $\mathbf{u}(x,r,\theta,t)$ is approximated as:

$$\mathbf{u}(x,r,\theta,t) = \langle \mathbf{u}(x,r,\theta,t) \rangle + \mathbf{u}'(x,r,\theta,t) = \langle \mathbf{u}(x,r,\theta,t) \rangle + \sum_{i=1}^{n_m} \psi^{(i)}(t)\sigma^{(i)}\phi^{(i)}(x,r,\theta) \tag{1}$$

with x, r and θ being the axial, radial and azimuthal coordinates, respectively, and t being the time coordinate. $\langle \mathbf{u}(x,r,\theta,t) \rangle$ and $\mathbf{u}'(x,r,\theta,t)$ indicate the time-averaged and the fluctuating part of the velocity field according to the Reynolds decomposition. The set of functions $\phi^{(i)}(x,r,\theta)$ constitute the basis of the spatial decomposition of the fluctuating velocity field, $\psi^{(i)}(t)$ constitutes the basis of the temporal decomposition

and σ_i are the magnitudes associated to each spatio-temporal mode; the symbol n_m indicates the number of modes.

The choice of the eigenfunctions performed by the POD in its snapshot formulation (Sirovich, 1987), aims at maximizing the correlation between the vectorial field $\mathbf{u}(\mathbf{x},t)$ and the function $\psi^{(i)}(t)$, i.e. it aims to minimize the projection residual of $\mathbf{u}(x,r,\theta,t)$ onto the set of functions $\psi^{(i)}(t)$. Moreover, the set of $\psi^{(i)}(t)$ functions are subjected to a mutual orthogonality constrain. The solution to this problem is given by the solution of the Fredholm equation, i.e. they are calculated as the eigenfunctions of the two-points temporal correlation tensor. Similarly it is possible to restate the entire problem to prove that the spatial basis $\phi^{(i)}(x,r,\theta)$ are the eigenfunctions of the temporally-averaged spatial correlation operator, retrieving the classic POD formulation (Lumley, 1967). The singular values σ_i which are associated to each temporal and spatial eigenfunction pair are therefore the square root of the correlation tensor eigenvalues and they are a measure of how much turbulent kinetic energy is associated to the spatio-temporal eigenfunction over the entire data ensemble.

4 Galerkin projection

In order to estimate the dynamics of the flow from non-time-resolved data, it will be assumed that the time derivative of the flow field in the close proximity of a time instant can be modelled according to the following advection equation:

$$\frac{\partial}{\partial t}\mathbf{u}(x,r,\theta,t) + (\mathbf{U_c}\cdot\nabla)\mathbf{u}(x,r,\theta,t) = 0 \tag{2}$$

where $\mathbf{U_c} = [U_{c,x}, U_{c,r}, U_{c,\theta}]$ is the convective velocity. Following Jaunet et al. (2016), a reduced order model of the flow dynamics can be obtained from a Galerkin projection of this equation into the space spanned by the POD eigenfunctions, which provides the temporal derivatives associated to each spatio-temporal mode of the POD:

$$\frac{\partial}{\partial t}\psi^{(i)}(t) = \sum_j \psi^{(j)}\sigma^{(j)}\left((\mathbf{U_c}\cdot\nabla)\phi^{(j)^T}(x,r,\theta)\right)\phi^{(i)}(x,r,\theta) = \sum_j \psi^{(j)}(t)L^{(j,i)}$$

$$L^{(j,i)} = \sigma^{(j)}\left((\mathbf{U_c}\cdot\nabla)\phi^{(j)^T}(x,r,\theta)\right)\phi^{(i)}(x,r,\theta) = \psi^{(j)^T}(t)\frac{\partial}{\partial t}\psi^{(i)}(t) \tag{3}$$

where $L^{(j,i)}$ measures the cross-contribution of different modes in the time derivative. For this work, a constant convection velocity $\mathbf{U_c} = [0.6\cdot U_J, 0, 0]$ has been selected, following typical results from literature (Lau et al., 1972).

A similar approach can be used to provide also information of the pressure field associated to each velocity-field structure. The pressure gradient can be modelled from the equation (White and Corfield, 2006):

$$\nabla p = -\rho\left(\frac{\partial}{\partial t}\mathbf{u} + (\mathbf{u}\cdot\nabla)\mathbf{u} - \nu\nabla^2\mathbf{u}\right) \approx -\rho\left(\frac{\partial}{\partial t}\mathbf{u} + (\mathbf{u}\cdot\nabla)\mathbf{u}\right) \tag{4}$$

The pressure equation can be projected onto the POD modes:

$$-\frac{1}{\rho}\nabla\phi_p^{(i)^T}(x,r,\theta) = \sum_j \sigma^{(i)^{-1}}\psi^{(i)^T}\frac{\partial}{\partial t}\psi^{(j)}(t)\sigma^{(j)}\phi^{(j)^T}(x,r,\theta)$$

$$+ \sum_m\sum_n \sigma^{(i)^{-1}}\psi^{(i)^T}\left(\left(\psi^{(m)}\sigma^m\phi^{(m)^T}(x,r,\theta)\cdot\nabla\right)\left(\psi^{(n)}\sigma^n\phi^{(n)^T}(x,r,\theta)\right)\right) \tag{5}$$

$$= \sum_j \sigma^{(i)^{-1}}L^{(i,j)}\sigma^{(j)}\phi^{(j)^T}(x,r,\theta) + \sum_m\sum_n \sigma^{(i)^{-1}}\psi^{(i)^T}\mathbf{Q}^{(m,n)}(x,r,\theta,t)$$

where the projection of the pressure fluctuation into the POD temporal eigenfuctions $\phi_p^{(i)}((x,r,\theta) = p'^T(x,r,\theta,t)\psi^{(i)}(t)\sigma^{(i)^{-1}}$ can be considered as the part of the pressure fluctuations correlated to each velocity POD mode. The last term of Eq. 5 measures the cross-contribution of 3 velocity modes on the pressure modes.
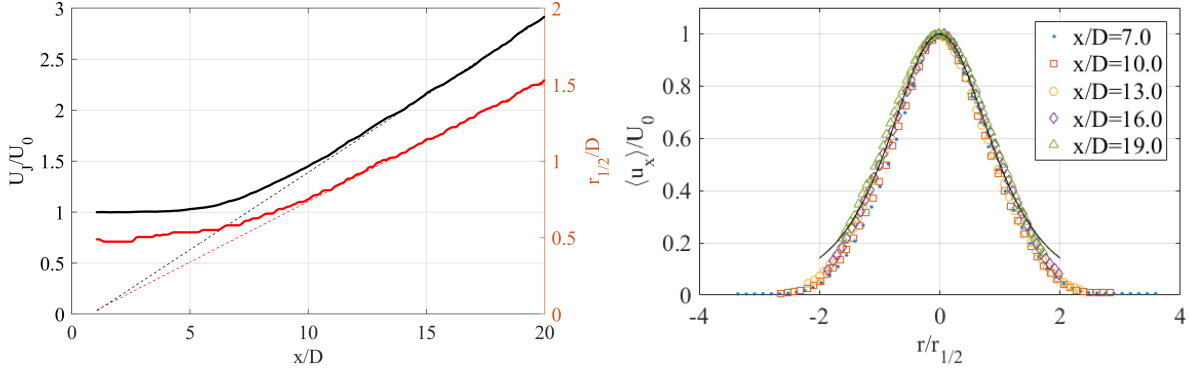
Figure 2: Left: centerline velocity and jet half-width along the axial direction. Right: time-averaged axial velocity profiles. Black solid line is the approximated theoretical model of self-similar axial velocity profile as reported in Pope (2001).

5 Jet characterization

The time-average flow in the jet symmetry plane is extracted from the 2600 instantaneous PIV velocity fields. Fig. 2 reports the evolution along the axial direction of the local centerline velocity $U_0(x) = \langle u_x(x, r = 0) \rangle$ and of the jet half-width $r_{1/2}(x)$, defined as the point in which $\langle u_x(x, r_{1/2}) \rangle = 0.5 U_0(x)$. Both the quantities shows an approximately linear behaviour starting from $x/D \approx 8$. In order to check the quality of the jet flow and of the measurements, the curves have been linearly fitted in the range $x/D \in [15, 20]$ according to the asymptotic solutions reported in Pope (2001):

$$\frac{U_0}{U_J} = \frac{B}{\frac{x}{D} - \frac{x_0}{D}}$$
$$\frac{r_{1/2}}{D} = S \left(\frac{x}{D} - \frac{x_0}{D} \right)$$

(6)

The fitting resulted in values of the parameters equal to $S \approx 0.08$, $B \approx 6.5$ and $\frac{x_0}{D} \approx 0.84$. It should be noted that the discrepancies with respect to values reported in the literature for the asymptotic case (Pope, 2001) are relatively small, despite being calculated for much lower axial distance from the nozzle. The time-averaged axial velocity profiles at different distances from the nozzle is also shown in Fig. 2. The velocity has been rescaled with the local centerline velocity U_0 in the jet centerline, while the radial coordinate has been rescaled with the local half-width $r_{1/2}$ of the jet. The measured velocity profiles have been reported alongside the theoretical model of the self-similar axial velocity profile (Pope, 2001) for comparison:

$$\frac{\langle u_x \rangle}{U_0} = \frac{1}{1 + a\eta^2}$$
$$a = \frac{\sqrt{2} - 1}{S^2}$$
$$\eta = S \frac{r}{r_{1/2}}$$

(7)

The time-averaged velocity profiles reported show that the jet does not present any relevant asymmetry. Indeed the velocity profiles reported do not perfectly match with the self-similar solution due to the limited extension of the measurement domain ($y/D < 30$).

6 Decomposition results

The Proper Orthogonal Decomposition has been applied to extract coherent features in the jet. Given the axial symmetry of the flow conditions, it is possible to expect that the instantaneous flow field possesses
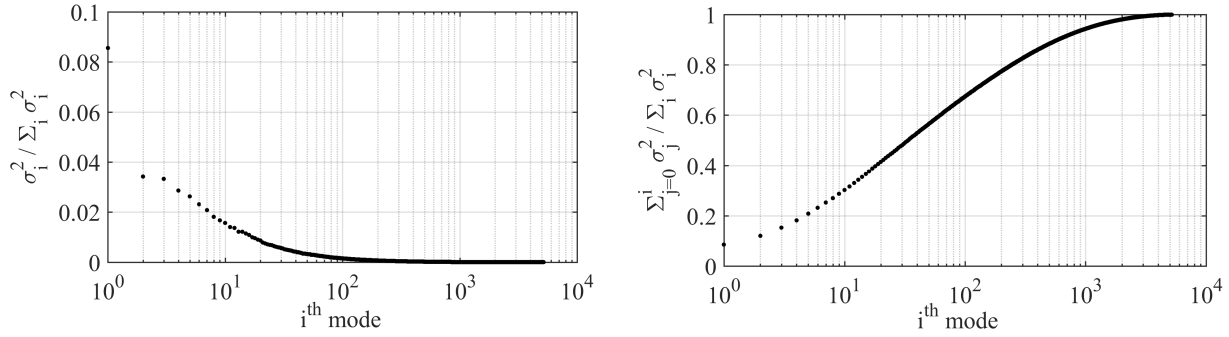
Figure 3: Left: POD energy spectrum. Right: cumulative POD energy spectrum.

circular symmetry. Therefore the azimuthal direction of the field can be considered as an homogeneous direction, i.e. differences between two points along the azimuthal direction only depends on the distance between them (Holmes et al., 2012). In these conditions the decomposition in the azimuthal direction should lead simply to Fourier azimuthal modes. In order not to pollute the decomposition in the inhomogeneous directions (both axial and radial) and preserve the symmetries of the flow field (Aubry et al., 1993), the POD is applied only to half of the measured domain along the radial direction. To increase the number of snapshots fed to the decomposition and to obtain more statistically converged modes, the other half of the domain, mirrored along the jet axis, has been included in the ensemble of snapshots of the velocity field.

Fig. 3 reports the eigenvalues of the two-point cross-correlation matrix, i.e. the energy POD spectrum, calculated over the entire measured flow-field domain. The plot shows that the kinetic energy spreads over a large quantity of modes. Only the first mode contains a relevant fraction of the energy (slightly more than 8% of the total). The rest of the modes shows a very low energy contribution, in line with the observations on the wave-packets energy reported in literature. Since the main focus of this work is aimed to large scale structures, the Galerkin projection of the advection and pressure equations has been computed accounting only for the first 50 modes, which approximately corresponds to an "elbow" in the POD eigenvalues graph according to the *scree test* (Cattell, 1966). It is worth remarking that the firsts 50 modes gather slightly more than 50% of the turbulent kinetic energy of the ensemble.

Fig. 4 reports the top 7 most energetic POD spatial modes (left column) and the associated pressure modes computed from the Galerkin projection (right column). As can be observed, the first mode represents a streak-like structure of high/low axial momentum. The pressure fluctuation associated to this mode, according to the Galerkin projection, has not a clear modal behaviour and is generally low. Most of the higher order POD modes shows a clear wavy-like structure along the axial direction, for $y/D > 6$, i.e. after the end of the potential core region, which seems to follow the jet spreading. The modes, however, do not represent an homogeneous wave but shows a clear intensity modulation in the axial direction, as observed in literature for wave-packets. This intensity modulation has been highlighted in Fig. 4 with a black solid line over the contour. The position of the maximum in the modulation envelope seems to be related both to the axial wavelength and to the local width of the jet: longer wavelength modes (typically lower order POD modes) have maximum intensity farther downstream, where jet width is larger. A possible interpretation for this is that the local size of the most energetic feature roughly corresponds to the jet width. It is worth remarking that, despite, the modes present similar turbulent structures displaced at different axial positions, it is not possible to recover any clear frequency or time-delay relationship using the Lissajous plots of pair of temporal modes. As shown in the Galerkin projection, in fact, the dynamics of each turbulent features in the field depends on all the other modes, thus resulting in the non-linearity of the phenomenon. The pressure fluctuation modes shows the modulated sinusoidal behavior already observed for the velocity modes, which seems to confirm the wave-packet nature of the recovered modes. Pressure fluctuation, however, seems to extend much further in the radial direction than their velocity counterpart. This is compatible with the figure of wave-packet pressure fluctuations that strongly affects the acoustic-near-field of the jet.

7 Conclusions

The present work reports a post-processing strategy to extract information on the dynamics of jet wave-packets from non-time-resolved velocity fields. Low-repetition-rate 2D-PIV measurements have been per-
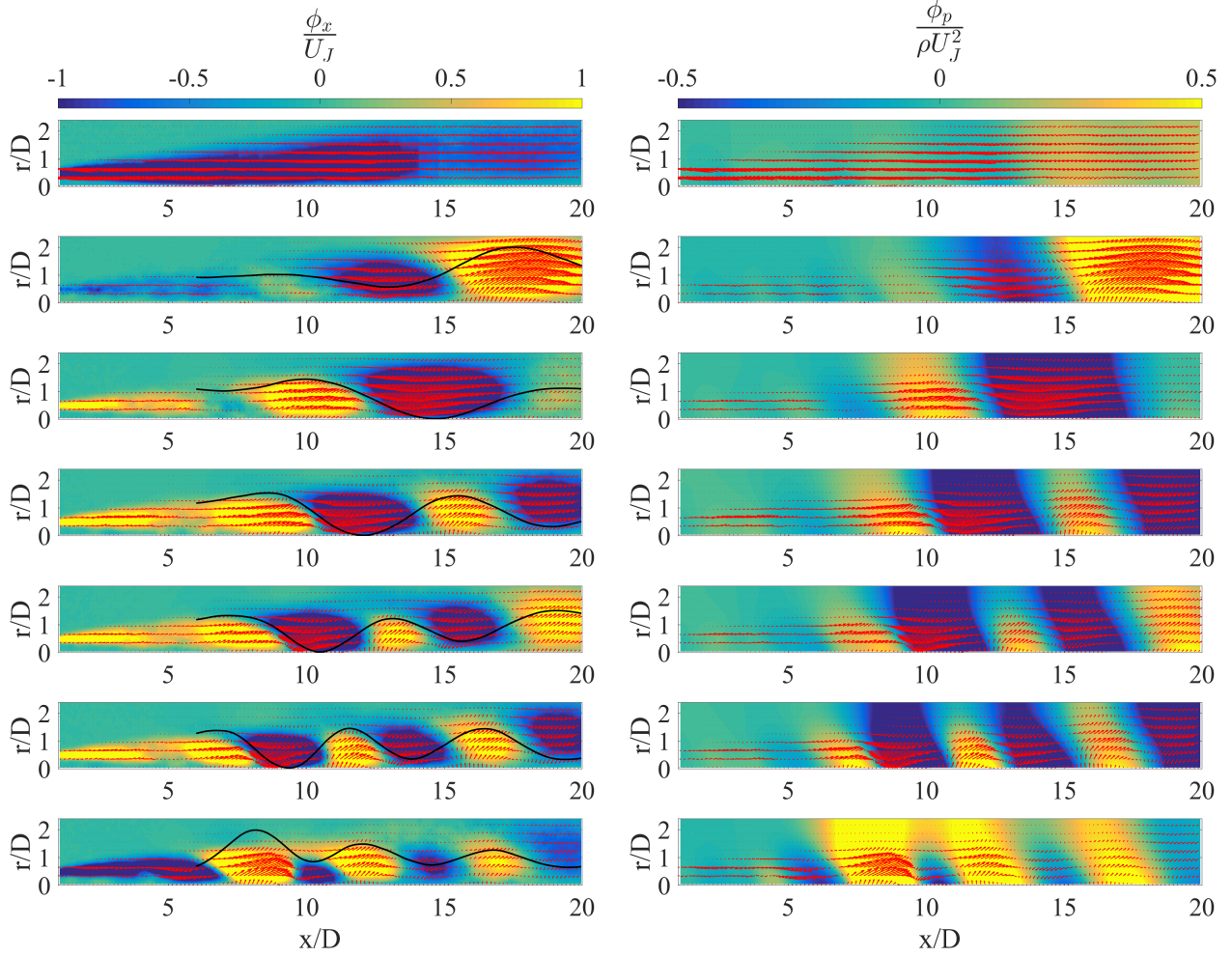
Figure 4: First 7 POD modes ranked (from top to bottom) by their kinetic energy contribution. Contour plot represents the axial velocity component (left) and the associated pressure fluctuations (right). Black solid line emphasizes the modulation of the structures in the axial direction.

formed in the symmetry plane of a subsonic turbulent round jet at $Re_D = 33000$. Ensemble-average statistics of the jet have been checked to verify that the measured flow field is symmetric with respect to the jet axis. Relying on the symmetry of the flow field, POD has been performed on the flow field halved with respect to the jet axis, in order to provide a set of spatial eigenfunction in the $x - r$ plane describing large-scale velocity structures in the jet. The flow-structure dynamics has been estimated through the Galerkin projection of an advection model, while the associated hydrodynamic pressure fluctuations has been obtained through Galerkin projection of the pressure equation. The velocity/pressure structures which have been identified using this approach shows a clear modal behavior with an intensity modulation in the axial direction, which suggests that the flow structures extracted can be regarded as jet wave-packets.

The strategy applied proved to be effective in retrieving the dynamic behavior of jet wave-packets, which would not be generally available from low-speed measurements. Most importantly, the estimated dynamics open the path to the characterization of the acoustic emission of the wave-packet structures through the use of Lighthill's analogy, which will be explored in the future.

Acknowledgements

References

Aubry N (1991) On the hidden beauty of the proper orthogonal decomposition. *Theoretical and Computational Fluid Dynamics* 2:339–352

Aubry N, Lian WY, and Titi ES (1993) Preserving symmetries in the proper orthogonal decomposition. *SIAM Journal on Scientific Computing* 14:483–505

Berkooz G, Holmes P, and Lumley JL (1993) The proper orthogonal decomposition in the analysis of turbulent flows. *Annual review of fluid mechanics* 25:539–575

Cattell RB (1966) The scree test for the number of factors. *Multivariate behavioral research* 1:245–276

Crighton D and Huerre P (1990) Shear-layer pressure fluctuations and superdirective acoustic sources. *Journal of Fluid Mechanics* 220:355–368

Crow SC and Champagne F (1971) Orderly structure in jet turbulence. *Journal of Fluid Mechanics* 48:547–591

Holmes P, Lumley JL, Berkooz G, and Rowley CW (2012) *Turbulence, coherent structures, dynamical systems and symmetry*. Cambridge university press

Jaunet V, Collin E, and Delville J (2016) Pod-galerkin advection model for convective flow: application to a flapping rectangular supersonic jet. *Experiments in Fluids* 57:84

Jaunet V, Jordan P, and Cavalieri A (2017) Two-point coherence of wave packets in turbulent jets. *Physical Review Fluids* 2:024604

Jordan P and Colonius T (2013) Wave packets and turbulent jet noise. *Annual review of fluid mechanics* 45:173–195

Jordan P and Gervais Y (2008) Subsonic jet aeroacoustics: associating experiment, modelling and simulation. *Experiments in Fluids* 44:1–21

Lau J, Fisher M, and Fuchs H (1972) The intrinsic structure of turbulent jets. *Journal of Sound and Vibration* 22:379–406

Lighthill MJ (1952) On sound generated aerodynamically i. general theory. *Proceedings of the Royal Society of London Series A Mathematical and Physical Sciences* 211:564–587

Lumley JL (1967) The structure of inhomogeneous turbulence. in V Yaglom and V Tatarski, editors, *Atmospheric Turbulence and Wave Propagation*. pages 166–178. Nauka

Mankbadi R and Liu J (1984) Sound generated aerodynamically revisited: large-scale structures in a turbulent jet as a source of sound. *Philosophical Transactions of the Royal Society of London Series A, Mathematical and Physical Sciences* 311:183–217

Michalke A and Fuchs H (1975) On turbulence and noise of an axisymmetric shear flow. *Journal of Fluid Mechanics* 70:179–205

Pope SB (2001) *Turbulent flows*. IOP Publishing

Scarano F (2001) Iterative image deformation methods in piv. *Measurement science and technology* 13:R1

Schmidt OT, Towne A, Colonius T, Cavalieri AV, Jordan P, and Brès GA (2017) Wavepackets and trapped acoustic modes in a turbulent jet: coherent structure eduction and global stability. *Journal of Fluid Mechanics* 825:1153–1181

Sirovich L (1987) Turbulence and the dynamics of coherent structures. i. coherent structures. *Quarterly of applied mathematics* 45:561–571

Tam CK, Viswanathan K, Ahuja K, and Panda J (2008) The sources of jet noise: experimental evidence. *Journal of Fluid Mechanics* 615:253–292

White FM and Corfield I (2006) *Viscous fluid flow*. volume 3. McGraw-Hill New York